



# Diffusion from a line source deployed in a homogeneous roughness layer: interpretation of wind-tunnel measurements by means of simple mathematical models

P. Kastner-Klein<sup>a,b</sup>, E. Fedorovich<sup>a,c,\*</sup>

<sup>a</sup> *Institute for Hydromechanics, University of Karlsruhe, Germany*

<sup>b</sup> *School of Civil Engineering and Environmental Science, University of Oklahoma, CEC, 202 West Boyd, Norman, OK 73019-1013, USA*

<sup>c</sup> *School of Meteorology, University of Oklahoma, SEC, 100 East Boyd, Norman, OK 73019-1013, USA*

Received 16 January 2000; received in revised form 14 January 2001; accepted 24 September 2001

## Abstract

In wind-tunnel studies of atmospheric dispersion, the pollutant emission by traffic is usually considered as ground-level line source. The source performance under different flow conditions is therefore important for the adequate description of pollutant dispersion. The dispersion from a line source in the wind-tunnel model of the atmospheric boundary layer has been investigated in the present study. Specially conducted mean flow and turbulence measurements have proved the similarity between the wind-tunnel flow and the flow in the lower portion of the atmospheric boundary layer. Lateral and vertical distributions of mean concentration downwind of the source have been measured with varying source parameters and wind velocities. The concentration pattern has not revealed a significant dependence on the parameter variations. The wind-tunnel results have been further evaluated by means of analytical and numerical dispersion models. The evaluation has shown a good general agreement of measured and calculated concentration fields. Two alternative sets of equations with different parameterizations of eddy diffusivity and different values of the turbulent Schmidt number have been employed in the analytical model calculations. A better agreement with the wind-tunnel results has been achieved with a similarity-theory expression for eddy diffusivity rather than with the eddy diffusivity parameterization based on the conjugate-power-law formula. The numerical model has provided the best match for the wind-tunnel concentration data at large distances from the source. However, certain discrepancies between the wind-tunnel and numerical predictions have been marked out close to the source. © 2002 Elsevier Science Ltd. All rights reserved.

**Keywords:** Dispersion; Vehicle emissions; Surface layer; Numerical modeling; Analytical model

## 1. Introduction

In physical and numerical models of atmospheric dispersion, traffic emissions are commonly simulated by ground-level line sources with a homogeneous and constant emission rate along the source. An appropriate design of a line source is therefore an important

prerequisite for physical modeling of vehicle emission dispersion in atmospheric boundary layer wind tunnels.

In this paper, we present results from a wind-tunnel study of dispersion from a ground-level line source under crosswind conditions. The technical parameters of the employed line source have been similar to those proposed by Meroney et al. (1996), who discussed the source properties essential for ensuring a homogeneous and constant release of tracer gas from the source.

Our study has been aimed at evaluation of the source applicability for dispersion studies in boundary layer wind tunnels. The measured concentration distributions

\*Corresponding author.

E-mail addresses: pkklein@ou.edu (P. Kastner-Klein), fedorovich@ou.edu (E. Fedorovich).

have been analyzed based on comparisons with dispersion patterns calculated by analytical and numerical models of dispersion from a line source deployed in a homogeneous roughness layer.

The first of the employed models—an analytical dispersion model—can be considered as an extended Gaussian model of the passive constituent diffusion in a turbulent shear flow. Models of this type are reviewed in Pasquill and Smith (1983), and Huang (1979). The model combines statistical and  $K$ -theory approaches to calculate the concentration distribution downwind of a source. The well-known conventional Gaussian dispersion model, described, e.g. in Seinfeld (1986), is a special case of this model.

The second model used for interpretation of the wind-tunnel data is a numerical model based on a finite-difference approximation of the concentration balance equation with prescribed velocity and turbulent diffusivity profiles corresponding to the case of a neutrally stratified, homogeneous atmospheric surface layer.

## 2. Wind-tunnel modeling of dispersion from a line source

### 2.1. Parameters of wind-tunnel flow

Wind-tunnel measurements to be presented in this paper have been performed in the neutral atmospheric boundary layer tunnel of the University of Karlsruhe (NATUK) that has a 10.5-m long, 2-m wide, and 1-m high test section, and produces a maximum wind speed of  $20 \text{ m s}^{-1}$ . The tunnel is described in Bächlin and Plate (1988). The turbulent boundary layer flow in the NATUK is generated with the aid of homogeneously distributed roughness elements mounted on the floor of the tunnel and by vortex generators installed at the tunnel inlet. Measurements of mean flow and turbulence characteristics in the wind tunnel have been performed with hot-wire and laser Doppler velocimeters. In the left-hand Cartesian coordinate system associated with the flow, the longitudinal axis ( $oX$ ) is directed downwind,  $oY$  is the lateral axis, and  $oZ$  is the vertical one. The corresponding velocity components are denoted as  $u$ ,  $v$ , and  $w$ , respectively.

Similarity between the boundary layer flow in the wind tunnel and in the atmosphere is a fundamental requirement for physical modeling of atmospheric dispersion (Plate, 1999). In the main portion of the neutrally stratified atmospheric surface layer, the wind profile may be described by the well-known logarithmic (hereafter called log) law (Tennekes, 1982):

$$u(z) = \frac{u_*}{\kappa} \ln \frac{z}{z_0}, \quad (1)$$

where  $\kappa = 0.4$  is the von Kármán constant,  $u_*$  is the shear stress (or friction) velocity, and  $z_0$  is the roughness

length of the underlying surface. A similar wind profile must be reproduced in the wind-tunnel boundary layer flow. Usually, the region with the log flow profile extends up to 20% of the total boundary layer depth  $\delta$  in the tunnel. Geometric similarity between the atmospheric and wind-tunnel flows requires the ratio of roughness lengths to be equal to the geometric model scale (Plate, 1999).

In the engineering practice, the wind profile in the atmospheric boundary layer is often approximated also by the following power-law expression (Plate, 1999):

$$u(z) = a(z - d_0)^\alpha, \quad (2)$$

which includes as parameters the displacement height  $d_0$  and the profile exponent  $\alpha$  that depends on the underlying surface roughness. The value of  $\alpha$  typically lies between 0.1 (water surfaces) and 0.4 (urban areas). The coefficient  $a$  is determined by the wind velocity at a chosen reference height.

Power-law formulation (2) is more practicable for engineering applications than log-law (1). It is known to fit well wind profiles observed in the atmosphere and reproduced in wind tunnels. The main advantage of Eq. (2) is its validity in the broader range of heights than that of Eq. (1); in many instances it fairly approximates the wind profile far beyond the upper limit of the atmospheric surface layer. The similarity requirement in terms of the power-law approximation can be formulated as equality of power-law exponents for the full-scale and model wind profiles (Plate, 1999).

Fig. 1 shows a mean velocity profile (symbols) measured in the center of the NATUK test section ( $u_0 = 10 \text{ m s}^{-1}$  is the wind velocity at the boundary layer height  $\delta = 450 \text{ mm}$ ) compared with approximations of this profile by the power-law function (left plot) and log law (right plot). Both the theoretical curves represent the measured profile fairly well. The log law with  $z_0 = 0.8 \text{ mm}$  and  $u_* = 0.055u_0$  almost perfectly fits the lower part of the velocity profile up to the height  $z \approx 200 \text{ mm}$ . The parameters of the power-law profile that provides the best fit of experimental data in Fig. 1 are  $\alpha = 0.23$  and  $d_0 = 2 \text{ mm}$ . The value of the surface Reynolds number in the wind tunnel,  $Re_s = u_*z_0/\nu \approx 15$  (where  $\nu$  is the kinematic viscosity of the air), matches the criterion for the rough wall turbulent flow:  $Re_s \geq 5$  (Plate, 1982).

The rms values of velocity fluctuations in the wind-tunnel boundary layer are plotted in the left plot of Fig. 2. In the lower portion of the boundary layer, they are in good agreement with velocity fluctuation data from the atmospheric surface layer (Arya, 1988):  $\sigma_u/u_* \approx 2.5$ ,  $\sigma_v/u_* \approx 1.9$  and  $\sigma_w/u_* \approx 1.3$ . One may notice, however, that modeled velocity component variances as well as the turbulent momentum flux  $-\overline{uw}$  (see the central plot of Fig. 2) noticeably vary with height. This indicates that the observed turbulence regime is not in

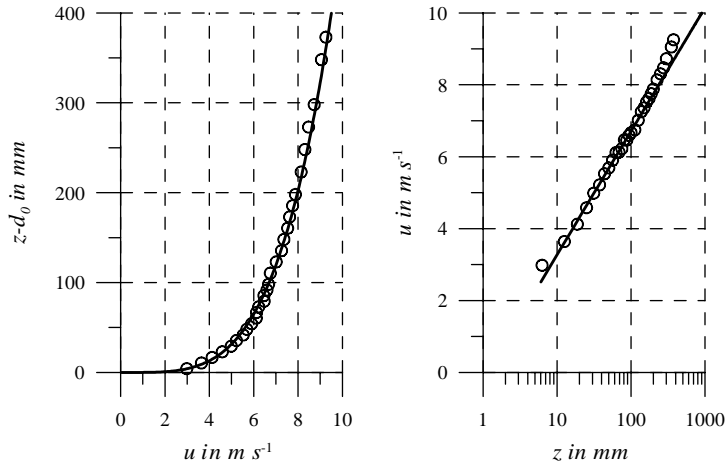


Fig. 1. Power-law (left diagram) and log-law (right diagram) approximations of the mean velocity profile measured in the wind-tunnel boundary layer (symbols).

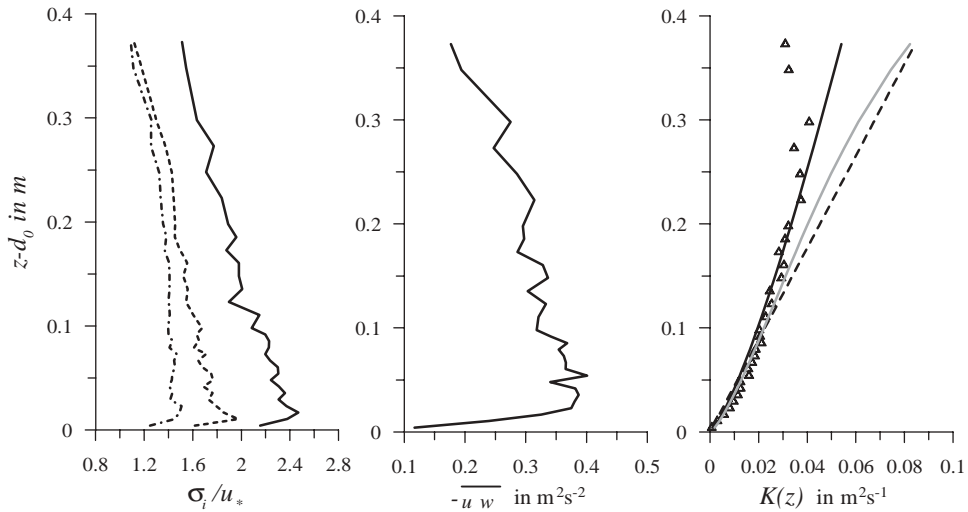


Fig. 2. Left plot: normalized velocity component rms fluctuations in the wind-tunnel flow; solid line shows  $\sigma_u$ , —  $\sigma_v$  and - - - -  $\sigma_w$ ; central plot: turbulent momentum flux  $-\overline{u'w'}$ ; right plot: turbulent diffusivity for momentum  $K_m(z)$  in the wind-tunnel flow (symbols) compared to the similarity theory (black dashed line) and conjugate-power law (black solid line)  $K_m(z)$  predictions. A turbulent diffusivity profile for a scalar,  $K_c(z)$ , calculated based on the conjugate-power-law expression for  $K_m(z)$  and  $Sc_t = 0.9 - 0.4(z/\delta)^2$  is shown by the gray line.

complete conformity with the constant stress layer assumption. In the right plot of Fig. 2, the turbulent diffusivity for momentum calculated from the wind-tunnel flux-profile measurements is compared with theoretical predictions. This comparison will be discussed in more detail in Section 3.

In addition to the presented flow parameters, a variety of other flow characteristics have been measured in the NATUK (Kastner-Klein, 1999) in order to evaluate the tunnel operating ranges for atmospheric dispersion studies. These measurements have demonstrated that,

alike the atmospheric spectra (Kaimal et al., 1972), the normalized velocity spectra at different heights in the wind-tunnel flow collapse roughly on one curve when scaled with the surface layer turbulence scales. Furthermore, the measured spectra were well represented by analytical relationships derived from atmospheric spectral data and feature clear, although rather short,  $-2/3$  law intervals in the high-frequency ranges.

The analysis of all relevant flow characteristics and their comparisons with atmospheric data allowed to

qualify the boundary layer flow in the NATUK as the scaled ( $M = 1:500$ ) analog of its atmospheric prototype.

## 2.2. Design of the line source

The line sources used in our study were constructed as proposed in Meroney et al. (1996), who found that the key characteristic influencing the gas flow from the source is the pressure drop through the exhaust holes. Meroney and colleagues achieved a high discharge pressure drop of 450 Pa for a flow rate  $1001 \text{ h}^{-1} \text{ m}^{-1}$  employing 25-mm long hypodermic pipes 0.25 mm in diameter. In our case, line sources of the length  $L_s = 1.42 \text{ m}$  were equipped with 25-mm long outlet pipes, each of internal diameter  $D = 0.5 \text{ mm}$ . The distance between the pipes along the source was 5 mm. The pipes were integrated in a chamber that was supplied with a mixture of air and tracer gas ( $\text{SF}_6$ ) through several inlet ports located along the source at 10-cm distance from each other. The tracer gas flow rate  $Q_t$  was much smaller than the airflow rate  $Q_a$ , so that the overall discharge rate could be regulated only by the airflow rate  $Q_a$ . The gas discharge velocities at the pipe outlets were up to  $1 \text{ m s}^{-1}$ . In order to minimize potential flow disturbances by such relatively high gas discharges, the source outlets were sheltered by 10-mm wide and 2-mm thick metal stripes that were laterally deflecting the vertical momentum of discharge. The distance between the outlets and the stripes was 2 mm.

## 2.3. Concentration fields downwind of the line source under crosswind conditions

To evaluate the line source performance, concentration distributions have been registered downwind of the source under crosswind conditions. The wind velocity and the gas flow rates have been varied in order to ascertain the lateral homogeneity of the source exhaust

for variable flow conditions and to ensure the Reynolds number independence of the normalized concentration fields. The values of the wind velocity  $u_0$  at boundary layer height  $\delta$  in the performed experiments have been set to equal 5, 7, 9, and  $12 \text{ m s}^{-1}$ . The source flow rate per unit length  $Q_a$  has been varied in the range from 37 to  $1491 \text{ h}^{-1} \text{ m}^{-1}$  that corresponds to a discharge velocity  $v_e$  variation from 0.25 to  $1.05 \text{ m s}^{-1}$ . Vertical concentration profiles at nine positions ranging from 22.5 to 900 mm along the centerline of the tunnel, and lateral profiles at two distances from the source,  $x = 90 \text{ mm}$  and 180 mm, have been measured for each combination of  $u_0$  and  $Q_a$ . Concentration values at ground level in the wind tunnel are locally affected by individual roughness elements and are therefore not representative. Due to that, concentration has been evaluated at  $z = 10 \text{ mm}$ .

In Figs. 3 and 4 we show concentration measurement results from four test experiments with  $Q_a = 1491 \text{ h}^{-1} \text{ m}^{-1}$  and  $u_0 = 5 \text{ m s}^{-1}$  ( $\times \times$ ),  $Q_a = 741 \text{ h}^{-1} \text{ m}^{-1}$  and  $u_0 = 5 \text{ m s}^{-1}$  ( $\triangle \triangle$ ),  $Q_a = 741 \text{ h}^{-1} \text{ m}^{-1}$  and  $u_0 = 7 \text{ m s}^{-1}$  ( $\diamond \diamond$ ), and  $Q_a = 741 \text{ h}^{-1} \text{ m}^{-1}$  and  $u_0 = 9 \text{ m s}^{-1}$  ( $\circ \circ$ ). Before being plotted, the measured tracer gas concentration  $c$  has been normalized as

$$c^* = \frac{cu_{\text{ref}}z_{\text{ref}}}{Q_t/L_s}, \quad (3)$$

where the wind velocity  $u_0$  at the boundary layer height has been used as reference velocity  $u_{\text{ref}}$ , and the boundary layer height  $\delta = 450 \text{ mm}$  as reference height  $z_{\text{ref}}$ . The ratio  $Q_t/L_s$  [ $\text{L}^2 \text{ T}^{-1}$ ] describes the tracer gas flow rate per unit length.

As the first test criterion of the source performance, the lateral variability of the concentration field has been considered, see Fig. 3. The standard deviation of the presented crosswind concentration distribution is about 8% of the mean concentration, which is slightly higher than in the experiments of Meroney et al. (1996). However, the normalized concentration values in the plot do not show systematic dependence on the source

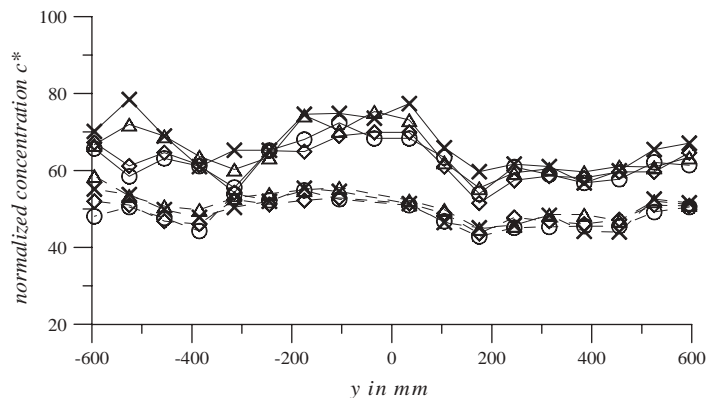


Fig. 3. Comparison of lateral concentration distributions measured in the height  $z = 10 \text{ mm}$  at  $x = 90 \text{ mm}$  (solid lines) and 180 mm (—) for four test cases with variable wind velocities and source flow rates; see the text for details.

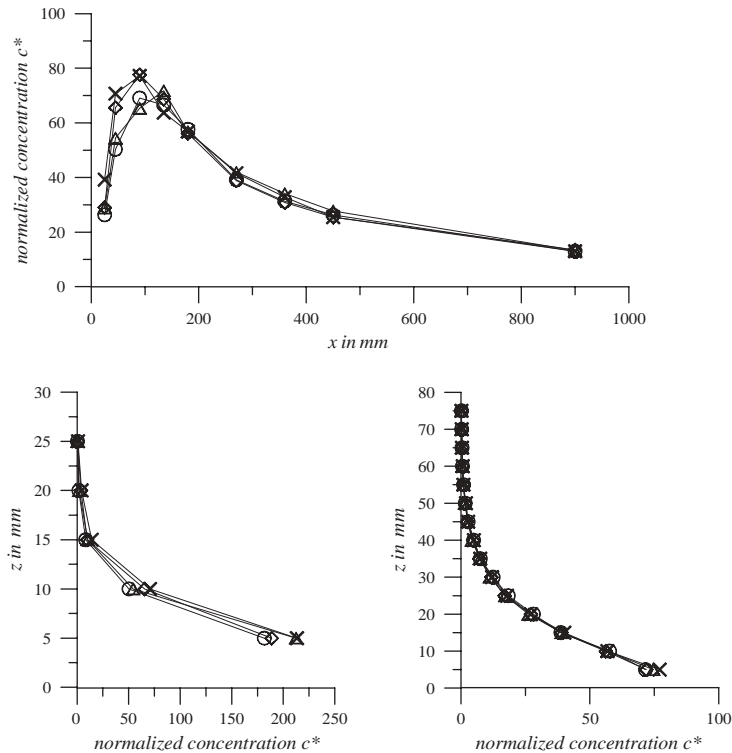


Fig. 4. Comparison of normalized longitudinal concentration distributions measured in the height  $z = 10$  mm (upper diagram) and vertical concentration profiles measured at  $x = 45$  mm (lower left diagram) and  $180$  mm (lower right diagram) downwind of ground-level line source for four test cases with variable wind velocities and source flow rates; see the text for more details.

strength and wind velocity. Also, the lateral variability of concentration is not markedly affected by changes of these test parameters. In additional tests with the sources placed inside street canyons (Kastner-Klein, 1999), the lateral variations of  $c^*$  have been found to be significantly smaller than those in Fig. 3. This suggests that the  $c^*$  variability in the present study is mainly caused by imprecise sampling heights and lateral inhomogeneity of the wind-tunnel flow rather than by source deficiencies or velocity disturbances due to gas discharge from the source.

In addition to lateral concentration distributions, we have analyzed the vertical concentration profiles and longitudinal variations of the near-ground concentration downwind of the source. The results are presented in Fig. 4. Close to the source, the main part of the plume is located below the sampling height  $z = 10$  mm, so that longitudinal concentration profiles first increase with distance, until a maximum value is reached at about  $100$  mm downwind of the source. In the near-source region, the normalized concentration values referring to the four test cases slightly diverge. It should be taken into account that the sampling point locations were readjusted for each test and due to the strong vertical concentration gradients, small inaccuracies in the

sampling point location could cause the observed divergence. The longitudinal profiles (upper plot) and vertical profiles at  $x = 180$  mm (lower right plot) demonstrate that the parameter variations had practically no influence on the downwind concentration distribution at larger distances from the source. The measured values from the four test cases collapse almost on one curve.

Summarizing the results of the test experiments, we may conclude that the constructed line source matches the basic requirements of vehicle emission dispersion modeling and ensures the Reynolds number independence of the concentration fields downwind the source. The wind-tunnel experimental data have been further analyzed by means of mathematical dispersion models presented in the next section.

### 3. Mathematical models of dispersion from line sources

#### 3.1. Analytical model

A detailed description of an analytical solution of the diffusion equation for the case of turbulent shear flow is given in Huang (1979). The solution is based on the

power-law approximation of the wind velocity profile  $u(z)$ , see Eq. (2), and an analogous representation of the turbulent diffusivity:

$$K_c(z) = b z^\beta. \quad (4)$$

For an infinite ground-level line source under crosswind conditions, the model yields a modified Gaussian function for the 2D concentration distribution, which can be formulated in terms of normalized concentrations according to Eq. (3):

$$c^*(x, z) = \underbrace{A(p, n) u_{\text{ref}} z_{\text{ref}} x^{-n}}_{c_0^*(x)} \exp\left(-\frac{z^p}{B(x)}\right) \quad (5)$$

with the exponent

$$p = 2 + \alpha - \beta \quad (6)$$

and the vertical dispersion parameter

$$B(x) = \frac{b}{a} p^2 x. \quad (7)$$

The auxiliary variables  $A(p, n)$ ,  $n$ , and  $v$  are expressed in terms of the present paper by

$$A(p, n) = \frac{p}{a^v (bp^2)^n \Gamma(n)}, \quad n = (1 + \alpha)/p, \\ v = (1 - \beta)/p.$$

If the wind profile is given by the log law, see Eq. (1), the parameters  $a$ ,  $\alpha$ ,  $b$ , and  $\beta$  of the velocity and eddy diffusivity profiles can be related to the roughness length  $z_0$  and a wind velocity  $u_{\text{ref}}$  at a reference height  $z_{\text{ref}}$ . This reference height is taken at the matching level of the power- and log-law profiles with respect to both wind velocity and its vertical gradient. The shear stress velocity can then be expressed as

$$u_* = \frac{\kappa u_{\text{ref}}}{\ln(z_{\text{ref}}/z_0)} \quad (8)$$

and the parameters of the power-law wind profile as

$$a = \frac{u_{\text{ref}}}{(z_{\text{ref}})^\alpha}, \quad (9)$$

$$\alpha = \frac{u_*}{\kappa u_{\text{ref}}} = \frac{1}{\ln(z_{\text{ref}}/z_0)}. \quad (10)$$

For the profile of eddy diffusivity  $K_c(z)$  for a scalar, which is related to the eddy diffusivity  $K_m(z)$  for momentum as  $K_c(z) = K_m(z)/Sc_t$ , where  $Sc_t$  is the turbulent Schmidt number, two alternative expressions are considered in Huang (1979). The first of them which is called the similarity-theory formulation is

$$K_c(z) = \kappa u_* z / Sc_t. \quad (11)$$

The second expression, that is the so-called conjugate-power-law formulation,

$$K_c(z) = \frac{1}{Sc_t} \frac{u_*^2}{\alpha} z^{1-\alpha} \quad (12)$$

is derived using the assumption of constant shear layer and the power-law approximation of the wind profile, Eq. (2). Depending on the choice of the eddy diffusivity expression, different values for the exponents  $p$  and  $n$  of concentration distribution (5) can be obtained. Formulation (11) gives  $p = 1 + \alpha$  and  $n = 1$  while formulation (12) yields  $p = 1 + 2\alpha$  and  $n = (1 + \alpha)/(1 + 2\alpha)$ . Both sets of parameters have been used to calculate concentration distributions for comparison with the wind-tunnel measurement data.

The results presented in the right plot of Fig. 2 show that the turbulent diffusivity profile  $K_m(z)$  derived from the wind-tunnel data is in better agreement with a conjugate-power-law formulation than with the similarity-theory prediction. For the turbulent diffusivity of scalar,  $K_c(z)$ , experimental data have not been available. In order to evaluate the relationship between  $K_m(z)$  and  $K_c(z)$  in the wind-tunnel experiments, the values  $Sc_t = 1$  and 0.7 have been tested. The first value corresponds to the commonly used assumption of equality between eddy diffusivity for mass and momentum in neutrally stratified turbulent flows, whereas the second value was found by Hassid (1983) to yield a better agreement between experimental results and analytical model predictions.

Recently, Koeltzsch (2000) found  $Sc_t$  to be a function of height in a neutrally stratified wind-tunnel flow. He observed a maximum of  $Sc_t \approx 0.95$  at  $z/\delta \approx 0.3$ , with  $Sc_t$  decreasing in the upper portion of the boundary layer and in the near-surface region. The latter effect was probably due to the influence of large surface roughness elements. This is not the case in the present study. The results of Koeltzsch (2000) for the upper portion of the boundary layer agreed reasonably well with the Rotta (1964) expression for the height dependence of the turbulent Prandtl number  $Pr_t(z) = 0.9 - 0.4(z/\delta)^2$ . Since our data are not suited to verify the height dependence of  $Sc_t$ , we have not taken this dependence into account in the dispersion model, but will comment on its relevance to our experimental data in Section 4.

### 3.2. Numerical model

We consider the diffusion of pollutant in the plane  $ZoX$  oriented perpendicular to the source, which is located at  $x = 0$  and  $z = 0$ . The source is taken to be of infinite length in the  $y$  direction. The concentration balance equation is used in the form:

$$u(z) \frac{\partial c}{\partial x} = \frac{\partial}{\partial z} K_c(z) \frac{\partial c}{\partial z} + I_s, \quad (13)$$

where  $c$  is the concentration,  $K_c$  is the coefficient of turbulent diffusion, and  $I_s$  is the source function. It is assumed that the flow regime is stationary, horizontal turbulent transport may be neglected, and both  $u$  and  $K_c$  are functions of  $z$  only. In the case of a horizontally

homogeneous surface layer, implicit expressions for these functions follow from the log-layer theory. The velocity profile is given by Eq. (1) and the turbulent diffusivity is expressed as in Eq. (11).

The concentration balance equation is solved numerically with boundary conditions  $\partial c/\partial z = 0$  at  $z = z_0$  (the concentration flux through the surface is assumed to be zero), and  $c = 0$  at  $z = \delta_1$ , which is the upper boundary of the logarithmic sublayer. From the velocity  $u_1$  defined at  $z = \delta_1$  and  $z_0$ , which are both considered known parameters, the friction velocity is determined as

$$u_* = \kappa u_1 / \ln \frac{\delta_1}{z_0} \quad (14)$$

The source function  $I_s$  is expressed through the source strength  $Q_s$  (given in units of  $[L^2 T^{-1}]$ ) as

$$I_s = \frac{Q_s}{\Delta x_1 \Delta z_1}, \quad (15)$$

where  $\Delta x_1 \Delta z_1$  is the area of the first numerical grid cell adjacent to the source. Beyond this grid cell, the source function is set equal to zero.

The employed finite-difference algorithm for solving the concentration balance Eq. (13) is implicit over  $x$  and uses the factorization method for integration over  $z$ .

#### 4. Comparison of wind-tunnel data with mathematical model predictions

For the inter-comparison of wind-tunnel, analytical, and numerical model data, the test case with  $Q_a = 1051 \text{ h}^{-1}$  and  $u_0 = 5 \text{ m s}^{-1}$  (see Section 2.3) has been chosen, and the wind profile has been described by the parameters  $\alpha = 0.23$  and  $z_0 \cong 0.4 \text{ m}$  (full-scale value). The measured and calculated concentration values have been normalized according to Eq. (3). The reference height  $z_{\text{ref}}$  was set equal to 60 mm (30 m in the nature). This height was estimated as matching level of the power- and log-law approximations of the mean velocity profile in the wind-tunnel boundary layer. Therefore, the normalized concentration values presented in this section are defined as  $c^* = cu_{60} 60 \text{ mm } L_s / Q_1$ .

To ensure consistency of the wind-tunnel data, we have checked the similarity of the vertical concentration profiles measured at nine different distances from the source corresponding to values from 12.5 up to 450 m in the nature. The near-ground concentration  $c_0^*(x)$  in the wind tunnel has been evaluated by data extrapolation from the two lower measurement levels  $z_1 = 5 \text{ mm}$  and  $z_2 = 10 \text{ mm}$ :

$$\begin{aligned} c_0^*(x) &= c^*(z_1) + \frac{\Delta c}{\Delta z} z_1 \\ &= c^*(z_1) + \frac{c^*(z_1) - c^*(z_2)}{z_2 - z_1} z_1. \end{aligned} \quad (16)$$

The vertical dispersion parameter  $B(z)$  and the power exponent  $p$  of the wind-tunnel concentration distribution have been obtained by the least mean square method from

$$\ln(c^*(x)/c_0^*(x)) = -1/B(x) z^p. \quad (17)$$

The values of exponent  $p$  have been found to vary within a range of 1.24–1.56 depending on the distance from the source, with a mean value  $\bar{p} = 1.33$ .

In Fig. 5, the normalized concentration data from the wind-tunnel (symbols) are presented versus normalized height  $z^{\bar{p}}/B(x)$ . The experimental data collapse practically on one curve in the main portion of the flow and display a good agreement with a modified Gaussian profile with  $p = 1.33$  (line). Towards the ground, however, the scatter between the experimental and analytical data slightly increases. This is apparently due to the inaccuracy of  $c_0^*(x)$  evaluation using Eq. (16) and higher sensitivity to sampling point deviations in regions with strong gradients. The mean value  $\bar{p} = 1.33$  lies well inside the range  $1.2 \leq p \leq 1.7$  for the full-scale concentration measurements summarized in Huang (1979). It is also close to the exponent  $p = 1.2$ , obtained in the wind-tunnel study of Meroney et al. (1986). The profile exponents calculated for the case of  $\alpha = 0.23$  by applying the similarity-theory and conjugate-power-law  $K_c(z)$  expressions, Eqs. (11) and (12), are  $p = 1.23$  and 1.46, respectively.

The results for the concentration distribution parameters, ground-level concentration  $c_0^*(x)$  and vertical

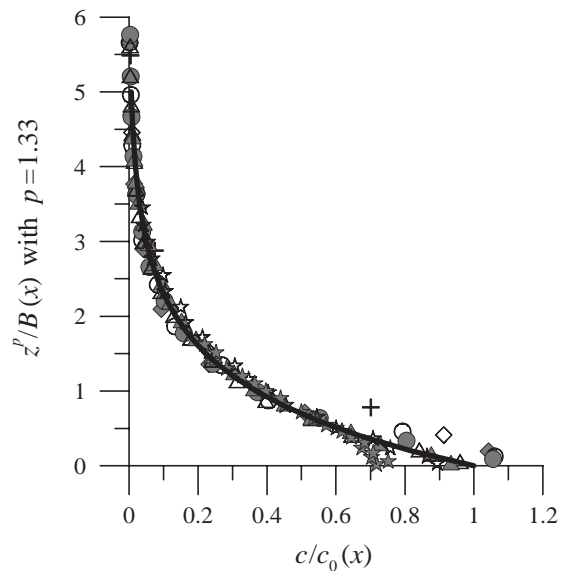


Fig. 5. Comparison of normalized vertical concentration profiles measured in the wind tunnel at nine different distances from the source, symbols, with a concentration profile predicted by an analytical dispersion model of Huang (1979), solid line.

Table 1

Comparison of concentration field parameters in the wind-tunnel model with predictions by analytical model of Huang (1979) using two alternative eddy diffusivity formulations

	Wind-tunnel data fit	$K_c$ after Eq. (11) with $Sc_t = 1$	$K_c$ after Eq. (12) with $Sc_t = 1$
Profile exponent	$p = 1.33$	$p = 1.23$	$p = 1.46$
Ground concentration	$c_0(x) \cong 284 x^{-0.86}$	$c_0(x) \cong 657 x^{-1}$	$c_0(x) \cong 193 x^{-0.84}$
Vertical dispersion parameter	$B(x) \cong 0.14 x^{1.09}$	$B(x) \cong 0.12 x$	$B(x) \cong 0.38 x$

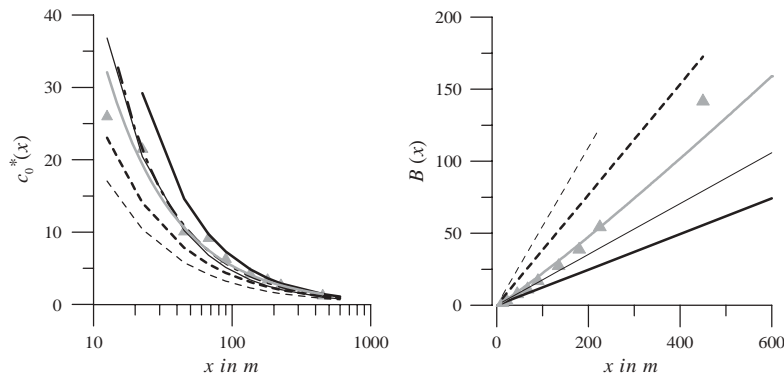


Fig. 6. Dependence of ground-level concentration (left plot) and vertical dispersion parameter (right plot) on the distance  $x$  from the source. Wind-tunnel data (gray symbols and lines) are compared with analytical model predictions alternatively based on Eq. (11), black solid lines, and Eq. (12), black dashed lines. Thick lines correspond to a turbulent Schmidt number  $Sc_t = 1$  and thin lines to  $Sc_t = 0.7$ . Numerical model data for  $Sc_t = 1$  are shown by - - - - -.

dispersion parameter  $B(x)$ , derived from the experimental data together with the corresponding analytical expressions are summarized in Table 1 and plotted in Fig. 6. The best-fit curves for the experimental data (gray lines) are found in between the analytical curves obtained with similarity-theory (11) and conjugate-power-law formulations (12) for  $K_c(z)$ . The latter formulation results in approximately two times smaller  $c_0^*(x)$  values and three times larger  $B(x)$  values than predicted using the similarity-theory formulation. The change of the turbulent Schmidt number from  $Sc_t = 1$  to 0.7 causes in the case of the conjugate-power-law approach even larger differences between experimental and model results. For the similarity-theory approach, the  $c_0^*(x)$  and  $B(x)$  curves are closer to the experimental data, but the model calculations tend to fall below the experimental near-ground concentrations  $c_0^*(x)$ . The numerical model prediction of  $c_0^*(x)$ , also plotted in Fig. 6, is in good agreement with the wind-tunnel measurement data. The vertical dispersion parameter has not been estimated from the numerical data.

Similar concentration distribution parameters have been observed in the wind-tunnel study of Poreh and Cermak (1964). They found that the ground-level concentration  $c_0(x)$  changes with increasing distance as  $x^{-0.9}$ . This decently agrees with  $c_0(x) \propto x^{-0.86}$  in our case. For the longitudinal variability of dispersion parameter

$\lambda$ , which in terms of our paper corresponds to  $B(x)^{1/p}$ , their data provided  $\lambda \propto x^{0.8}$ . Our measurements give a very close estimate:  $\lambda \propto x^{0.82}$ .

Finally, a comparison of measured and calculated concentration profiles at three distances from the source is shown in Fig. 7. Close to the source, the near-surface concentration calculated with the analytical model based on the power-law formulation for  $K_c(z)$  with  $Sc_t = 1$  is about 50% lower than the concentration observed in the wind tunnel. On the other hand, concentration values obtained using the similarity-theory formulation for  $K_c(z)$  show good agreement with the experimental data for this flow region and for  $Sc_t = 1$ . The similarity-theory formulation with  $Sc_t = 0.7$  provides larger differences between measured and calculated profiles, since the near-ground concentrations are significantly underestimated.

As has been mentioned in Section 3, the turbulent diffusivity for momentum in the wind-tunnel flow is better described by a conjugate-power-law profile than by the similarity theory. This looks somehow inconsistent with the significantly better performance of analytical dispersion model with similarity-theory formulation for  $K_m(z)$  and  $Sc_t = 1$ . An explanation for this discrepancy might be associated with the height dependence of the turbulent Schmidt number. The gray line in the right plot of Fig. 2 corresponds to a turbulent

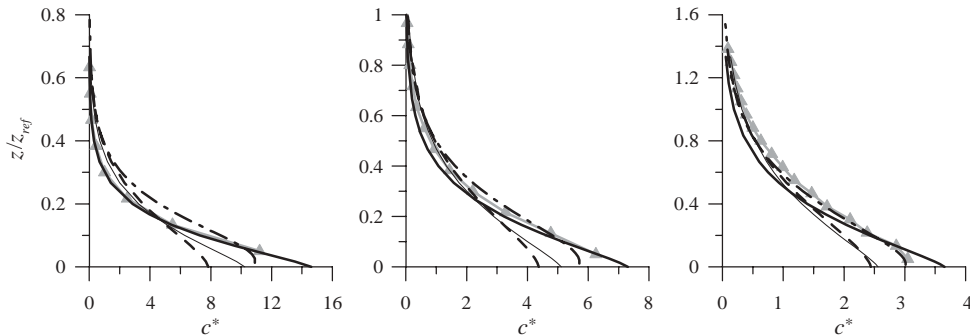


Fig. 7. Vertical concentration profiles at  $x = 45$  m (left plot),  $90$  m (central plot), and  $180$  m (right plot). Wind-tunnel results (gray symbols and lines) are compared with numerical (black dashed lines) and analytical (black solid lines) model predictions based on Eq. (11) with  $Sc_t = 1$ , and analytical model calculations with Eq. (12), black dashed lines. Thin black solid lines correspond to analytical model predictions based on Eq. (11) with  $Sc_t = 0.7$ .

diffusivity profile for scalar,  $K_c(z)$ , calculated with a conjugate-power-law profile for eddy viscosity  $K_m(z)$  and  $Sc_t = 0.9 - 0.4(z/\delta)^2$ . The latter expression is analogous to the  $Pr_t$  dependence on  $z$  proposed by Rotta (1964), see Section 3. One may notice that the resulting  $K_c(z)$  profile is very close to the  $K_m(z)$  profile predicted by the similarity theory (black dashed line). Thus, in our case the similarity theory complemented with assumption  $Sc_t = 1$  provides basically the same turbulent diffusivity for scalar as the conjugate-power law with  $Sc_t = 0.9 - 0.4(z/\delta)^2$ . This result, however, does not directly indicate that  $Sc_t$  significantly differs from 1 and depends on  $z$ . Additional studies are needed to investigate and understand this dependence.

The numerical model with  $Sc_t = 1$  overestimates the vertical mixing at small  $x$  and predicts slightly lower ground-level concentration compared to the wind-tunnel data. This inconsistency is presumably associated with inaccuracy of the source term  $I_s$  parameterization in the concentration balance Eq. (13). With increasing distance from the source, the vertical dispersion in the wind-tunnel flow becomes noticeably larger than predicted by the analytical model, and the best agreement with experimental results is provided by the numerical model.

## 5. Conclusions

The analysis of the turbulent flow in the wind-tunnel boundary layer and comparison with atmospheric data have demonstrated that flow profiles in the tunnel are in good agreement with those of the neutral atmospheric boundary layer scaled with  $M = 1 : 500$ .

The measurements of vertical and lateral concentration profiles downwind of the line source under variable source conditions and with different wind velocities allowed to evaluate the performance of the constructed line source. The measurement data have shown that the

requirement of laterally homogenous and constant release of tracer gas along the source was fulfilled. Flow field disturbances by gas discharges have been minimized, and the Reynolds number independence of the measured concentration distributions has been proved.

The performed inter-comparison of wind-tunnel and mathematical model data has revealed good quantitative correspondence between measured and calculated concentration distributions in the atmospheric surface layer downwind of a ground-level line source. The similarity of wind-tunnel concentration profiles measured at different distances downwind of the line source has been demonstrated. The shape of the normalized concentration profile in the wind tunnel agrees well with analytical predictions. The value of profile exponent  $p$  derived from the wind-tunnel data reasonably corresponds to its theoretical and experimental estimates published in the literature. The data inter-comparison has confirmed the acceptability of the constructed line source for the dispersion modeling purposes.

The inter-comparison has also shown that similarity-theory formulation for eddy diffusivity incorporated in analytical dispersion models provides more realistic concentration patterns than the alternative power-law formulation. The model calculations based on the latter formulation have been consistently underestimating ground-level concentration values compared to the data provided by other experimental and model methods. The differences observed between calculations with these two alternative formulations of eddy diffusivity are more significant than differences related to variations of the  $z$ -constant turbulent Schmidt number in the range from 0.7 to 1. Further studies are necessary to investigate the height dependence of  $Sc_t$ . At this point, we would abstain from any straightforward recommendation concerning the appropriate value of the turbulent Schmidt number in the neutrally stratified boundary layer flow.

## Acknowledgements

The reported study was supported by the Air Pollution Prevention Measures Programme (PEF) jointly funded by the Land of Baden-Württemberg (Germany) and the European Commission, and by the TRAPOS project of the TMR Programme of the European Commission.

## References

- Arya, S.P., 1988. Introduction to micrometeorology. Academic Press, San Diego, CA, 305pp.
- Bächlin, W., Plate, E.J., 1988. The dispersion of accidentally released gases in a built-up area. *Energy and Buildings* 11, 163–169.
- Hassid, S., 1983. Turbulent Schmidt number for diffusion models in the neutral boundary layer. *Atmospheric Environment* 17, 523–527.
- Huang, C.H., 1979. A theory of dispersion in turbulent shear flows. *Atmospheric Environment* 15, 453–463.
- Kaimal, J.C., Wyngaard, J.C., Izumi, Y., Coté, O.R., 1972. Spectral characteristics of surface layer turbulence. *Quarterly Journal of the Royal Meteorological Society* 98, 563–689.
- Kastner-Klein, P., 1999. Experimentelle Untersuchung der strömungsmechanischen Transportprozesse in Straßenschluchten, (Experimental investigation of fluid mechanical transport processes in street canyons). Ph.D. Thesis, University of Karlsruhe, Germany.
- Koeltzsch, K., 2000. The height dependence of the turbulent Schmidt number within the boundary layer. *Atmospheric Environment* 43, 1147–1151.
- Meroney, R.N., Pavageau, M., Rafailidis, S., Schatzmann, M., 1996. Study of line source characteristics for 2D physical modelling of pollutant dispersion in street canyons. *Journal of Wind Engineering and Industrial Aerodynamics* 62, 37–65.
- Pasquill, F., Smith, F.B., 1983. *Atmospheric Diffusion* (3rd Edition). Ellis Horwood Series in Environmental Sciences. Ellis Horwood, Chichester, UK, 437pp.
- Plate, E.J., 1982. Wind tunnel modelling of wind effects in engineering. In: Plate, E.J. (Ed.), *Engineering Meteorology*. Elsevier, Amsterdam, pp. 573–639.
- Plate, E.J., 1999. Methods of investigating urban wind fields—physical models. *Atmospheric Environment* 33, 3981–3989.
- Poreh, M., Cermak, J.E., 1964. Study of diffusion from a line source in a turbulent boundary layer. *International Journal of Heat and Mass Transfer* 7, 1083–1095.
- Rotta, J.C., 1964. Temperaturverteilungen in der turbulenten grenzschicht an der ebenen platte. *International Journal of Heat and Mass Transfer* 7, 215–228.
- Seinfeld, J.H., 1986. *Atmospheric Chemistry and Physics of Air Pollution*. Wiley-Interscience Publication, Wiley, New York, 738pp.
- Tennekes, H., 1982. Similarity relations, scaling laws and spectral dynamics. In: Nieuwstadt, F.T.M., van Dop, H. (Eds.), *Atmospheric Turbulence and Air Pollution Modelling*. D. Reidel, Dordrecht, pp. 37–68.